Estimating satellite orbital drag during historical magnetic superstorms

Denny M. Oliveira[1,2], Eftyhia Zesta[2], Hisashi Hayakawa[3,4], Ankush Bhaskar[2,5]

[1]Goddard Planetary Heliophysics Institute, University of Maryland, Baltimore County, Baltimore, MD United States

[2]NASA Goddard Space Flight Center, Greenbelt, MD United States

[3]Graduate School of Letters, Osaka University, Toyonaka, 5600043, Japan (JSPS Research Fellow)

[4]UK Solar System Data Centre, Space Physics and Operations Division, RAL Space, Science and Technology Facilities Council, Rutherford Appleton Laboratory, Harwell Oxford, Didcot, Oxfordshire, OX11 0QX, United Kingdom

[5]Catholic University of America, Washington, D.C. United States

Key Points:

- Historical magnetic superstorms (minimum Dst $\leq$ –500 nT) occurred before CHAMP's and GRACE's operation times
- Standard Dst and equivalent Dst data are used by the JB2008 empirical model to estimate extreme orbital drag effects
- Interplay between storm-time duration and minimum Dst and Dst-like values determine the severity of satellite drag effects in low-Earth orbit

Abstract

Understanding extreme space weather events is of paramount importance in efforts to protect technological systems in space and on the ground. Particularly in the thermosphere, the subsequent extreme magnetic storms can pose serious threats to low-Earth orbit (LEO) spacecraft by intensifying errors in orbit predictions. Extreme magnetic storms (minimum Dst $\leq$ –250 nT) are extremely rare: only 7 events occurred during the era of spacecraft with high-level accelerometers such as CHAMP (CHAllenge Mini-satellite Payload) and GRACE (Gravity Recovery And Climate experiment), and none with minimum Dst $\leq$ –500 nT, here termed magnetic superstorms. Therefore, current knowledge of thermospheric mass density response to magnetic superstorms is very limited. Thus, in order to advance this knowledge, 4 historical magnetic superstorms, i.e., events occurring before CHAMPs and GRACEs commission times, are used to empirically estimate density enhancements and subsequent orbital drag. The November 2003 magnetic storm (minimum Dst = –422 nT), the most extreme event observed by both satellites, is used as the benchmark event. Results show that, as expected, orbital degradation is more severe for the most intense storms. Additionally, results clearly point out that the time duration of the storm is strongly associated with storm-time orbital drag effects, being as important as or even more important than storm intensity itself. The most extreme storm-time decays during CHAMP/GRACE-like sample satellite orbits estimated for the March 1989 magnetic superstorm show that long-lasting superstorms can have highly detrimental consequences for the orbital dynamics of satellites in LEO.

Plain Language Summary

We investigate drag effects on satellites orbiting Earth in its upper atmosphere during magnetic storms caused by the impacts of solar superstorms. During magnetic storms, the upper atmosphere is heated and expands upwards, resulting in increased drag forces on satellites flying in those regions. Enhanced drag effects directly impact operations of such spacecraft, for instance, orbital tracking and predictions, maneuvers, and lifetime maintenance. The U.S. Federal Government has recognized space weather phenomena as natural hazards, and the understanding of their consequences, particularly during extreme circumstances, is of paramount importance. The very extreme events, here termed magnetic superstorms, occurred before the space era when no in-situ observations of the atmospheric density are available. Therefore, we use an empirical model to estimate drag from these historical events. Results generally show that the most extreme events drive the most severe effects. Additionally, we show that another storm feature, its time duration, can play a significant role in enhancing drag. Therefore, we argue that space weather forecasters should be aware of events with long duration, particularly the ones caused by sequential impacts of solar disturbances on the Earths magnetic field, when predicting and forecasting the subsequent drag effects on satellites in the upper atmosphere.

1 Introduction

Magnetic storms are global phenomena that occur due to the interaction of solar perturbations with the Earth's magnetosphere (Gonzalez et al., 1994). The most intense and severe magnetic storms are commonly caused by coronal mass ejections (CMEs) (Gonzalez et al., 1994; Daglis et al., 1999; Balan et al., 2014). CMEs usually have a shock at their leading edge that is promptly followed by a sheath and a magnetic cloud (Gonzalez et al., 1994; Balan et al., 2014; Kilpua et al., 2019). Extreme magnetic storms are caused by the impact of extremely fast CMEs on the Earth's magnetosphere (Tsurutani & Lakhina, 2014), usually associated with highly depressed values of the southward component of the interplanetary magnetic field (Gonzalez et al., 1994; Daglis et al., 1999; Balan et al., 2014; Tsurutani & Lakhina, 2014; Kilpua et al., 2019).

Extreme space weather events like severe magnetic storms have been recognized by the U.S. Federal Government through the National Space Weather Strategy and Action Plan (National Science and Technology Council, 2015b, 2015a) as a natural hazard, and the need to establish benchmarks for extreme space weather events has also been recognized by the scientific community (e.g., Lanzerotti, 2015; Jonas et al., 2017; Riley et al., 2018). The intensity of magnetic storms is usually measured by depletions of the ground horizontal magnetic field component recorded by magnetometers located at mid- and low-latitudes by means of the disturbance storm time (Dst) index (section 2.1). Extremely severe events, here termed magnetic superstorms, with minimum Dst $\leq$ –500 nT, are notably rare (Cliver & Dietrich, 2013; Riley et al., 2018; Vennerstrøm et al., 2016; Hayakawa, Ebihara, Willis, et al., 2019; Chapman et al., 2020). For instance, the March 1989 event, the only superstorm occurring during the space age (Meng et al., 2019), is well-known for the occurrence of low-latitude aurorae (Allen et al., 1989; Rich & Denig, 1992; Pulkkinen et al., 2012) and intense geomagnetically induced currents (GICs) which caused the blackout of the Hydro-Québec system in Canada for several hours, leading to serious economic losses (Bolduc, 2002; Kappenman, 2006; Pulkkinen et al., 2017). However, though arguably, the most extreme ground horizontal magnetic field perturbation ($\sim$ –1600 nT) on record was recorded by the Colaba station during the Carrington event of September 1859 (Tsurutani et al., 2003; Siscoe et al., 2006; Hayakawa, Ebihara, Willis, et al., 2019). Since that is the only known low-latitude data set available to date, a global analysis of that storm cannot be performed (Siscoe et al., 2006; Cliver & Dietrich, 2013; Hayakawa, Ebihara, Willis, et al., 2019; Blake et al., 2019). For this reason, the Carrington event is not addressed in this paper.

During active times, large amounts of electromagnetic energy enter the ionosphere-thermosphere system causing the prompt thermosphere heating and upward extension due to mechanical collisions between ions and neutrals (e.g., Prölss, 2011; Emmert, 2015). This energy has access to the thermosphere primarily through high latitudes (Fuller-Rowell et al., 1994; Liu & Lühr, 2005; Huang et al., 2014; Connor et al., 2016; Lu et al., 2016; Kalafatoglu Eyiguler et al., 2018), and propagates equatorward due to the occurrence of gravity waves and wind surges (Fuller-Rowell et al., 1994; Hocke & Schlegel, 1996; Bruinsma & Forbes, 2007; Sutton et al., 2009). Therefore, the heating and upwelling of the thermosphere are global phenomena (Richmond & Lu, 2000; Liu et al., 2005; Sutton et al., 2009). As a result, satellites that happen to fly in those regions experience increased effects of drag forces leading to their subsequent orbital degradation (Prölss, 2011; Prieto et al., 2014; Zesta & Huang, 2016). The understanding and control of orbital drag effects during active times can enhance predictability and forecasting of satellite tracking, reentry processes, and maintenance of satellite life times (Prölss, 2011; Zesta & Huang, 2016; Berger et al., 2020), particularly during extreme magnetic storms (Oliveira & Zesta, 2019). Most of these studies have used data obtained from state-of-the-art accelerometers onboard two low-Earth orbit (LEO) satellites, namely CHAMP (CHAllenge Minisatellite Payload; Reigber et al., 2002) and GRACE (Gravity Recovery And Climate Experiment; Tapley et al., 2004). These spacecraft were launched after 2001 (section 2.2).

The most extreme magnetic storm experienced by CHAMP and GRACE took place in November 2003 with minimum Dst = –422 nT. Consequently, there are no assessments of satellite drag in LEO during magnetic superstorms inferred from high-accuracy accelerometer data. The orbital degradations of CHAMP and GRACE associated with the November 2003 event during stormy times were, respectively, $\sim$ –285 m and $\sim$ –71 m (Krauss et al., 2015; Oliveira & Zesta, 2019), much more severe than the natural drag caused by the quiet-time backgorund density estimated by Oliveira and Zesta (2019), namely –34.45 m and –6.86 m, respectively. Hence, these are the most extreme orbital decays measured with high-quality accelerometer data. In order to empirically estimate drag effects during magnetic superstorms, standard Dst data and ground magnetometer data of historical superstorms reconstructed from historical archives are used by a thermospheric empirical model (section 2.3) for density computations (section 2.4). These

122 events occurred in March 1989 (Allen et al., 1989; Boteler, 2019), with the traditional
123 Dst index available, September 1909 (Silverman, 1995; Hayakawa, Ebihara, Cliver, et al.,
124 2019), May 1921 (Silverman & Cliver, 2001; Hapgood, 2019), and October/November
125 1903 (Lockyer, 1903; Ribeiro et al., 2016), with an alternative version to the Dst index
126 available. Effects of storm time duration associated with minimum values of Dst and Dst-
127 like data will be estimated and compared. As a result, this effort will improve our un-
128 derstanding of severe satellite orbital drag effects in LEO caused by magnetic superstorms.

2 Data, model, and a framework for orbital drag estimations

2.1 Disturbance storm time indices

131 In this study, magnetic activity is represented by the Dst index provided by the
132 World Data Center for Geomagnetism, Kyoto et al. (2015). This 1-hr-resolution index
133 was defined in 1957, the International Geophysical Year (IGY), as described by Sugiura
134 (1964). Specifically, Dst is computed by averaging latitudinally weighted horizontal mag-
135 netic field perturbations, with a background removal scheme, recorded by mid- and low-
136 latitude stations with reasonably even longitudinal separation according to the expres-
137 sion

$$Dst = \frac{1}{4}\sum_{i=1}^{4}\frac{\Delta H_i}{\cos\Lambda_i}, \quad i \text{ in [HON, SJG, HER, KAK]} \tag{1}$$

138 where ΔH_i is the horizontal magnetic perturbation of the i-th station, and Λ_i is the con-
139 temporary magnetic latitude of the i-th station. The colored stars in Figure 1 show the
140 stations, with their corresponding names, abbreviations, and geographic locations, used
141 to compute standard Dst after the IGY.

142 Additionally, recent efforts have been undertaken to provide alternative (but sim-
143 ilar) versions to the standard Dst index for historical magnetic superstorms with archival
144 material. The events took place in October/November 1903 (Hayakawa et al., 2020), Septem-
145 ber 1909 (Love et al., 2019b), and May 1921 (Love et al., 2019a). This alternative in-
146 dex, also with resolution of 1 hr, was reconstructed with data obtained from 4 low/mid-
147 latitude stations, with the best possible longitudinal separation, and is represented here
148 by Dst†. The corresponding contemporary magnetic latitudes were computed by the au-
149 thors. A background removal scheme similar to the one used to calculate Dst is used in
150 the source papers as well. The stations used to compute Dst† used in this study are shown
151 by the colored crosses in Figure 1. Therefore, the Dst† index is given by

$$Dst^{\dagger} = \frac{1}{4}\sum_{j=1}^{4}\frac{\Delta H_j}{\cos\Lambda_j}, \quad j \text{ in } \begin{cases} \text{[CLA, COI, CUA, ZKW]} & \text{for Oct/Nov 1903} \\ \text{[API, MRI, SFS, VQS]} & \text{for Sep 1909} \\ \text{[API, SFS, VSS, WAT]} & \text{for May 1921} \end{cases} \tag{2}$$

152 The Dst† data for the magnetic superstorms used here are available as supporting
153 information provided by the respective references (Hayakawa et al., 2020; Love et al., 2019b,
154 2019a). Details of individual stations and magnetograms for each corresponding Dst†
155 network is provided in the source articles.

2.2 Neutral mass density data

157 CHAMP and GRACE neutral mass density (ρ) data obtained from their respec-
158 tive high-accuracy accelerometers are used in this work. CHAMP was launched in 2001
159 at the initial altitude 456 km and orbital inclination 87.25°. It covered each 1 hr local
160 time in 5.5 days with orbital period 90 min. The GRACE-A and -B spacecraft were launched

Figure 1. Geographic locations of the ground magnetometer stations that compose the standard Dst network that has been used by the World Data Center for Geomagnetism, Kyoto et al. (2015) since 1957 (colored stars), and the alternative Dst† network used by Hayakawa et al. (2020), Love et al. (2019b), and Love et al. (2019a) for the historic events of October/November 1903, September 1909 and May 1921 (colored crosses), respectively. Magnetic latitudes (solid cyan lines) and magnetic equator (solid orange line) were computed by the Altitude-Adjusted Corrected Geomagnetic Coordinates Model (Shepherd, 2014) for 1957. Note that the SJG and VQS stations are very close to each other.

in 2002 at the initial altitude 500 km and orbital inclination 89.5°. The GRACE constellation covered each 1 hr local time in 6.7 days with orbital period 95 min. GRACE-A flew ∼220 km ahead of GRACE-B. As discussed in Oliveira and Zesta (2019), only GRACE-A data are used, henceforth GRACE data, because GRACE-A data show higher quality than GRACE-B data. CHAMP re-entered in 2010, while GRACE re-entered in 2018. Uncertainties and calibration techniques of both missions have been discussed by many papers (e.g., Bruinsma et al., 2004; Doornbos & Klinkrad, 2006; Flury et al., 2008).

The density data used in this study are normalized and intercalibrated as described in Oliveira et al. (2017) and Zesta and Oliveira (2019). Basically, the Jacchia-Bowman 2008 (hereafter JB2008, Bowman et al., 2008, see below) empirical model computes quiet-time densities (ρ_0) in order to obtain the background state for the quiet thermosphere. This approach ensures that the ratio and the difference between the storm-time and quiet-time densities are as close to one ($\rho/\rho_0 \approx 1$) and zero ($\rho - \rho_0 \approx 0$) as possible, respectively. As a result, storm-time density enhancements can be extracted more effectively (Oliveira et al., 2017; Oliveira & Zesta, 2019; Zesta & Oliveira, 2019).

2.3 The Jacchia-Bowman 2008 (JB2008) empirical model

The JB2008 empirical model computes thermospheric density from a single parameter, the exospheric temperature (see equation 2 in Oliveira & Zesta, 2019). This temperature depends on several satellite parameters such as latitude, local time, and altitude. Additionally, this model uses the solar radio flux at wavelength 10.7 cm, indicated by the F10.7 index, to account for thermospheric heating due to solar UV radiation (Bowman et al., 2008). Finally, a term that depends on Dst in the exospheric temperature represents the magnetic activity contribution. Dst and Dst† data of the historical magnetic superstorms recorded by the stations shown in Figure 1 will be used along with LEO satellite orbital data during the event of November 2003 to estimate drag effects. A description of the JB2008 model along with other popular thermospheric empirical models has recently been provided by He et al. (2018).

2.4 Orbital drag computations

Neutral mass densities are derived by high-accuracy accelerometers according to the drag equation (Prieto et al., 2014):

$$a_d = -\frac{1}{2}\rho C_D \frac{S}{m}V^2 \quad V = |\vec{V}_{s/c} - \vec{V}_{wind}|, \tag{3}$$

where a_d is the spacecraft acceleration caused by drag forces; ρ is the local thermospheric neutral mass density; C_D is the drag coefficient; S/m is the area-to-mass ratio; and V is the relative velocity between the spacecraft velocity ($\vec{V}_{s/c}$) and the ambi-

Figure 2. CHAMP (left-hand-side column) and GRACE (right-hand-side column) orbits, in magnetic coordinates, for the northern hemisphere (top row) and southern hemisphere (bottom row). The colorbars represent the corresponding altitudes during the time interval 19-23 November 2003, the benchmark event chosen for this study. The grey arrows in all panels indicate CHAMP's and GRACE's trajectories in both hemispheres.

ent neutral wind velocity ($\vec{V}_{wind}$). In this equation, all quantities are presumably known, and therefore it is solved for ρ in order to yield density. However, these parameters (particularly C_D) can introduce significant errors in density computations (Moe & Moe, 2005; Prieto et al., 2014; Zesta & Huang, 2016). In this study, drag coefficients computed with error mitigation methods by Sutton (2009) were used.

Chen et al. (2012) provide the following expression for the computation of storm-time orbital decay rate:

$$\frac{da}{dt} = -C_D \frac{S}{m} \sqrt{GM\langle a \rangle} \Delta\rho \,, \tag{4}$$

with a being the semi-major axis of the satellite orbit (temporal Earth's radius plus satellite altitude, Oliveira & Zesta, 2019), $G = 6.67 \times 10^{-11}$ m$^3 \cdot$kg$^{-1} \cdot$s^{-2} the gravitational constant, $M = 5.972 \times 10^{24}$ kg the Earth's mass, and $\Delta\rho$ the difference between the modeled storm-time and quiet-time densities. The daily average of the semi-major axis a is represented by $\langle a \rangle$.

Finally, the storm-time orbital decay is computed by the sum over all da/dt values along the satellite's path for any (t_1, t_2) interval:

$$d(t) = \int_{t1}^{t2} a(t)dt \tag{5}$$

3 Results

3.1 The selected magnetic superstorms

The benchmark event for the current study occurred in November 2003. That storm had minimum Dst = –422 nT, the most intense magnetic storm event with both CHAMP and GRACE neutral mass density data available. Ground magnetometer data and neutral mass density data for the GRACE satellite are shown in Figure 1 of Zesta and Oliveira (2019). The solar flux F10.7 index increased from 151 sfu (solar flux units) on 19 November to 175 sfu on 23 November (Liu & Lühr, 2005).

Figure 2 documents the orbits of CHAMP and GRACE in the time interval from 19 to 23 November 2003. The dial plots show orbits as a function of magnetic latitudes (MLATs) and magnetic local times (MLTs). The left column shows altitudes for CHAMP, while the right column shows altitudes for GRACE. The top row indicates data for the northern hemisphere, while the bottom row indicates data for the southern hemisphere. The colorbars indicate altitudes for both satellites in the same periods.

CHAMP is in a near noon-midnight orbit. The orbit altitudes of CHAMP increased at high latitudes and at the poles of both hemispheres and decreased at mid- and low-latitudes. Similar behavior is shown by GRACE whose orbits were confined within the

Figure 3. Ground magnetometer Dst and Dst† time series, with resolution of 1 hr, for the storms of (a) October/November 1903 (Dst†, Hayakawa et al., 2020); (b) May 1921 (Dst†, Love et al., 2019a); (c) March 1989 (Dst, World Data Center for Geomagnetism, Kyoto et al., 2015); and (d) September 1909 (Dst†, Love et al., 2019b). The highlighted regions correspond to the time span between storm sudden commencement (SSC, vertical dashed lines) and the beginning of the storm recovery phases (minimum Dst or Dst†), or time duration of storm development.

mid-noon/dusk and mid-midnight/dawn sectors. Therefore, both spacecraft provide reasonable coverage between the day and night sectors. The altitude variations shown in Figure 2 caused by density variations at different MLATs and MLTs are mitigated by the density intercalibration method introduced by Oliveira et al. (2017).

CME leading edges are usually associated with the occurrence of positive jumps in the Dst index, while its sudden depression is associated with the arrival of CME magnetic material or sheaths (e.g., Gonzalez et al., 1994; Kilpua et al., 2019). The first perturbation, termed storm sudden commencement (SSC), is caused by the shock compression (e.g., Oliveira et al., 2018; Shi et al., 2019), while the second event, termed storm main phase, is associated with strong driving of the magnetosphere via magnetic reconnection (e.g., Gonzalez et al., 1994; Daglis et al., 1999; Kilpua et al., 2019). Examples of SSCs and storm main phases represented by the Dst and Dst† indices during magnetic superstorms caused by fast CMEs are illustrated in Figure 3.

Figure 3 shows ground magnetometer time series for the magnetic superstorms of (a) October/November 1903 (Dst†); (b) May 1921 (Dst†); (c) March 1989 (Dst); and (d) September 1909 (Dst†). Data are plotted 12 hr and 72 hr around each respective SSC (dashed vertical black lines). Times are shown as Greenwich Mean Time (GMT) for all events, except as Universal Time (UT) for the 1989 event because UTs were introduced only in 1928 (Hapgood, 2019). Given the similarities of UTs and GMTs, here they will be used interchangeably (Hapgood, 2019). The highlighted areas of each panel correspond to the time interval between SSC and minimum Dst/Dst† occurrences, which also marks the beginning of the storm recovery phase. This time interval will henceforth be referred to as the storm development duration time in this paper.

Panels (a) and (b) show that the 1903 event is the weakest (minimum Dst† = –513 nT), whilst the 1921 event is the strongest (minimum Dst† = –907 nT) amongst all events. In contrast, the development duration times of both events are almost the same, $\sim$ 14 hr and $\sim$ 12 hr, respectively. Storm strengths can be estimated by computing how fast Dst (or Dst†) is depressed during storm development. The average slope of Dst/Dst† during the development phase is quantified by the difference of Dst/Dst† minimum minus Dst/Dst† peak at SSC compression by the development time. This provides a quantifiable measure of the impactfulness of the storm, meaning that storms with very low amplitude rates are commonly associated with high geomagnetic activity (e.g., Gonzalez et al., 1994). The estimated amplitude rates are –44.8 nT/hr and –80.0 nT/hr for the October/November 1903 and May 1921 events, respectively. These numbers explain why the effects of the 1921 event, such as equatorial extent of low-latitude aurorae (Chree, 1921; Silverman & Cliver, 2001), and GIC impacts on telegraph systems (Kappenman, 2006; Hapgood, 2019) were more severe than the effects of the 1903 event, mostly represented by mid-latitude aurorae (Page, 1903; Hayakawa et al., 2020), and local GIC impacts on contemporary telegraph systems in the United States and in the Iberian Peninsula (Ribeiro et al., 2016; Hayakawa et al., 2020).

On the other hand, the superstorms of March 1989 and September 1909 (panels c and d) had very similar minimum values for Dst and Dst†, around –590 nT. However,

Figure 4. JB2008 satellite orbital drag estimating results for the selected events for CHAMP's orbit (a1-d1) and GRACE's orbit (a2-d2) during the November 2003 event, but with hypothetical Dst/Dst† values. Panels a1/b1 and a2/b2: da/dt and d for the events in October/November 1903 (yellow lines) and May 1921 (green lines). Panels c1/d1 and c2/d2 indicate the same, but for the events in March 1989 (red lines) and September 1909 (blue lines). The highlighted areas correspond to the storm development duration, or the time interval between SSC occurrence and the end of the storm main phase (minimum Dst or Dst† occurrence).

the storm development duration of the 1989 event (24 hr) was 3 times longer than that of the 1909 event (8 hr). Consequently, the development amplitude rates of both superstorms were –23.8 nT/hr and –75.0 nT/hr, respectively. With respect to the aurorae of these events, Hayakawa, Ebihara, Cliver, et al. (2019) estimated, based on contemporary observations, that their equatorward extent reached ∼ 32° MLAT during the 1909 superstorm, as opposed to 40° MLAT estimated from particle precipitation measurements by satellites during the 1989 superstorm (Rich & Denig, 1992; Pulkkinen et al., 2012). Intense GICs occurred during both events, with several reports of geophysical disturbances on telegraph systems in 1909 (Silverman, 1995; Hayakawa, Ebihara, Cliver, et al., 2019; Hapgood, 2019; Love et al., 2019b), and on power transmission lines in 1989, particularly the power blackout in Québec, Canada (Allen et al., 1989; Kappenman, 2006; Oliveira & Ngwira, 2017; Boteler, 2019). During the 1989 event, the only event with satellite-based data amongst the four superstorms, the number of space objects "lost" in LEO increased dramatically around periods of maximum intensity due to errors introduced by storm heating effects into tracking systems (Allen et al., 1989; Joselyn, 1990; Burke, 2018). The left part of Table 1 summarizes these storm properties.

A comprehensive comparison of GIC effects caused by the superstorms on the contemporary ground infrastructure, i.e., telegraph systems and power grids, is a difficult task to be accomplished. However, the comparisons above show that the latitudinal extent of the auroral oval was more equatorward for the events with lower amplitude rates (May 1921 and September 1909 events). Next, the effects of these amplitude rates on storm-time orbital drag will be evaluated and compared for the 4 historical magnetic superstorms studied in this paper.

3.2 Storm-time orbital drag effects

Figure 4 shows results of storm-time satellite orbital drag effects estimated according to the framework presented in section 2.4. The computations are performed for the orbits of CHAMP and GRACE (Figure 2), with the orbital parameters the satellites had during the November 2003 storm. The sample CHAMP- and GRACE-like satellites are flown through an upper atmosphere produced by the JB2008 model for Dst/Dst† of the superstorms of Figure 3. All solar indices are kept the same, as those of the benchmark storm. For the sake of comparisons, results are plotted as a function of arbitrary times (GMT/UT) 12 hr before and 72 hr after the SSC onset as seen in Figure 3. The dashed vertical black lines (t = 0) indicate the times of SSC occurrence, while the highlighted areas correspond to the storm development duration as shown in Figure 3 for each corresponding storm.

The top 4 panels of Figure 4 (a1-d1) show results for CHAMP's orbit, while the bottom 4 panels (a2-d2) show results for GRACE's orbit. Panels a1 and a2 show storm-time orbital decay rates (equation 4) computed for the October/November 1903 superstorm (yellow line) and May 1921 superstorm (green line) for CHAMP and GRACE, respectively. Both events had approximately the same development times and very differ-

Table 1. Summary of the properties of the magnetic superstorms and subsequent orbital drag results shown in Figures 3 and 4, respectively.

Magnetic superstorm properties					Orbital drag effects		
Storm Month and year	SSC GMT/UT (Day)[a]	Min Dst/Dst[†] [nT]	Development duration[b] [hr]	Amplitude Rate[c] [nT/hr]	Satellite Name	Min da/dt [m/day]	Min d [m]
Oct/Nov 1903	0100(31)	−513	14	−44.8	CHAMP	−252.67	−102.65
					GRACE	−171.33	−65.39
May 1921	2300(14)	−907	12	−80.0	CHAMP	−432.98	−196.24
					GRACE	−319.43	−142.09
Mar 1989	0200(13)	−589	24	−23.8	CHAMP	−621.29	−388.59
					GRACE	−469.95	−305.58
Sep 1909	1200(25)	−595	8	−75.0	CHAMP	−285.14	−96.61
					GRACE	−191.25	−62.14

[a] Greenwich Mean Time or Universal Time and Day of Storm Sudden Commencement (SSC).

[b] Time between SSC and minimum Dst/Dst[†] occurrence.

[c] d(Dst/Dst[†])/dt

ent intensities (Table 1). The same is shown in panels c1 (CHAMP) and c2 (GRACE) for the superstorms of March 1989 (red line) and September 1909 (blue line). In this case, the storms had very similar intensities, but different development durations (Table 1). The storm-time orbital degradation (equation 5), is shown for CHAMP (panels b1 and d1) and GRACE (panels b2 and d2). The same colors used to represent da/dt results in panels a1/c1 and a1/c2 above are used to represent d results in panels b1/d1 and b2/d2.

Figure 4a1 shows that da/dt values during October/November 1903 for CHAMP were very close to zero before CME impact. On the other hand, da/dt values preceding the stormy period of May 1921 shows some oscillatory behavior, presumably linked to a similar behavior shown by ground magnetometer data during the same pre-storm period (Love et al., 2019b; Hapgood, 2019). CHAMP da/dt values for the 1921 event decreased faster in comparison to minimum da/dt values for the 1903 event. Similar orbital drag dynamics is observed for GRACE (a2), but the absolute values of the drag response are smaller (Table 1) because GRACE operated at higher altitudes in comparison to CHAMP (Krauss et al., 2018; Oliveira & Zesta, 2019). The da/dt results for CHAMP and GRACE are summarized in Table 1.

For the same pair of storms, the storm-time orbital degradations of CHAMP (panel b1) at the end of 72 hr after CME impact were –102.65 m and –196.24 m for both events, respectively. The same estimated results for GRACE (b2) are –65.39 m (1903) and –142.09 m (1921). Comparatively, the percentual difference between drag effects during both superstorms for CHAMP (91.17%) are higher than the percentual difference of the superstorm intensites (76.80%) most likely because the magnetosphere was hit by another CME on 16 May 1921 (Figure 3; Love et al., 2019a), leading to an additional magnetosphere energization during its recovery, which in turn impacted drag effects. Similarly, the orbital drag relative difference is higher in the case of GRACE (117.30%), when compared with the case of CHAMP. As suggested by Oliveira and Zesta (2019, Figure 10), this is presumably due to the interplay between heating propagation from auroral-to-equatorial latitudes and (possibly) the direct uplift of neutrals at low and equatorial latitudes more evident at altitudes higher than 400 km (Tsurutani et al., 2007).

In summary, the main features that arise from the comparison between these events are: (i) CHAMP and GRACE decayed faster during the most intense event (1921) due to its sharper negative excursion of the Dst[†] index and lower amplitude rate (Figure 3a

Table 2. Comparisons between magnetic superstorm intensity and satellite orbital drag severity for the magnetic superstorms in this study.

Magnetic Superstorm Month/Year	Comparisons between Superstorm intensities and durations	Relative differences of drag effects [%]			
		CHAMP		GRACE	
		da/dt	d	da/dt	d
Oct/Nov 1903 May 1921	May 1921 is 76.80% stronger Nearly the same durations	71.36	91.17	86.44	117.30
Sep 1909 Mar 1989	March 1989 is 3 times longer Nearly the same intensities	117.30	302.22	145.73	391.76
May 1921 Mar 1989	March 1989 is 2 times longer May 1921 is 53.98% stronger	43.49[a]	98.02	47.12	115.06

[a] Percentual differences between more severe (March 1989) with respect to less severe (May 1921) drag effects

and b; Table 1); and (ii) the relative differences between d for both events do not closely follow the relative differences between minimum Dst[†] values. This is likely the case because the magnetosphere was struck by another CME during its recovery, increasing the magnetospheric activity which in turn affected the subsequent orbital drag effects. Tables 1 and 2 summarize these results.

The comparisons between estimated drag effects for the March 1989 and September 1909 superstorms are remarkably different. These events had very similar strengths (similar minimum Dst and Dst[†] values), but their development times were quite distinct. Figure 4c1 shows that 1909 CHAMP da/dt values had a very sharp negative excursion after CME impact, which follows very closely the same feature in the Dst[†] index (Figure 3d). The minimum da/dt value (–285.14 m/day) for the September 1909 superstorm was reached shortly before minimum Dst[†]. On the other hand, the March 1989 drag effects are quite different, since da/dt decreased more slowly in comparison to the former case due to the differences in storm development amplitude rates. This is explained by the fact that the magnetosphere was most likely struck by multiple CMEs while the storm main phase was developing (Fujii et al., 1992; Lakhina & Tsurutani, 2016; Boteler, 2019). Similarly to the 1909 case, the minimum da/dt value (–621.29 m/day) occurred shortly before minimum Dst occurrence. The thermosphere recovery of the 1989 superstorm took longer than the thermosphere recovery of the 1909 superstorm, most likely because the magnetosphere was yet hit by more CMEs shortly after the beginning of the magnetosphere recovery (Figure 3c). A similar behavior is shown by the GRACE results, panel c2, but with smaller absolute values due to higher GRACE altitudes. The relative differences between da/dt peak values of CHAMP and GRACE for both superstorms are 117.30% and 145.73%, even though both events had approximately the same minimum Dst and Dst[†] values and very different storm development durations and amplitude rates.

Now the storm-time orbital degradations in both cases are evaluated. Figure 4d1 shows that CHAMP d decreased faster during the main phase of the 1909 event, reaching values near its minimum value around the beginning of storm recovery. This is a typical feature of drag effects triggered by a storm caused by an isolated CME (Krauss et al., 2015, 2018; Oliveira & Zesta, 2019). Conversely, CHAMP's orbital degradation decreased more dramatically during the recovery of the 1989 superstorm. These drag effects correlate well with a very sharp negative excursion presented by the Dst index, which is also directly related with the occurrence of low-latitude aurorae and very intense GICs around the world (Allen et al., 1989; Kappenman, 2006; Hayakawa, Ebihara, Cliver, et al., 2019). This time also coincides with the loss of orbital control of several objects in LEO as shown by satellite-based data (Allen et al., 1989; Joselyn, 1990; Burke, 2018). The storm-time orbital decays for the 1909 and 1989 events are –96.61 m and –388.59

m for CHAMP and –62.14 m and –305.58 m for GRACE. These orbital degradation levels were never observed by LEO spacecraft with high-precision accelerometers during magnetic superstorms, and therefore set a new base for drag effects under such circumstances. Their relative difference is 302.22% and 391.76%, closely following the proportion of storm time developments in the case of CHAMP. Taking into consideration that both superstorms were almost equally intense, these results show that the storm time duration can play a major role in driving orbital drag effects. Note also that relative differences are higher in the case of GRACE, most likely explained by the reasons suggested by Oliveira and Zesta (2019) as mentioned before.

Another striking difference concerning minimum Dst and Dst† values, storm development duration and subsequent amplitude rate impacts arises from the comparison between the May 1921 and March 1989 superstorms. The 1921 event was more than 50% stronger than the 1989 event, but active times during the latter lasted twice longer. The storm-time orbital decay for the March 1989 event was nearly twice more severe than the May 1921 event in both CHAMP's and GRACE's cases (Figure 4 and Tables 1 and 2). These results clearly reveal that a long-lasting magnetic superstorm can drive much more severe drag effects in comparison to a short-lasting, even stronger, superstorm. Tables 1 and 2 summarize the main results discussed in sections 3.1 and 3.2.

There are no solar wind nor interplanetary magnetic field data available for the magnetic superstorms discussed in this paper. Furthermore, it is important to emphasize that our statements concerning CME impacts are supported by our current knowledge of the underlying science: intense magnetic storms, particularly extreme events, are usually caused by CMEs (Gonzalez et al., 1994; Daglis et al., 1999; Balan et al., 2014; Tsurutani & Lakhina, 2014; Lakhina & Tsurutani, 2016; Kilpua et al., 2019).

4 Discussion and conclusion

Extreme magnetic storms (minimum Dst $\leq$ –250 nT) are very rare. Only 39 extreme events have taken place since the beginning of the space era (Meng et al., 2019), while only 7 extreme events were observed by CHAMP and GRACE (Oliveira & Zesta, 2019; Zesta & Oliveira, 2019). Additionally, only one magnetic superstorm (minimum Dst $\leq$ –500 nT) occurred since 1957, while none were ever observed by either CHAMP or GRACE. Therefore, current knowledge of thermospheric mass density response to magnetic supersotorms and the subsequent storm-time drag effects are very limited. Then, in order to estimate these effects, 4 historical magnetic superstorms were selected: one with standard Dst data (March 1989), and 3 with Dst† (Dst-like) data occurring on October/November 1903 (Hayakawa et al., 2020), September 1909 (Love et al., 2019b), and May 1921 (Love et al., 2019a). These Dst and Dst† data were used as input data for the JB2008 thermosphric empirical model for density computations. The extreme magnetic storm of November 2003 (minimum Dst = –422 nT), the most extreme event during CHAMP's and GRACE's commission times, was used as the benchmark event. The orbital drag framework provided by Oliveira and Zesta (2019) was used for drag estimations.

First, two events with different intensities but with approximately the same storm development times were compared (October/November 1903 and May 1921). Although the 1921 superstorm was $\sim$ 80% stronger than the 1903 superstorm, the drag effects in the former were up to 120% more severe than the effects in the latter (GRACE's case). This is attributed to the likely impact of another CME during the recovery phase of the 1921 superstorm. Second, the other pair of superstorms, with very similar strengths, but with the September 1909 storm development being 3 times shorter than the March 1989 storm development, were compared. Results show that the relative difference of the storm-time orbital degradation for the 1989 event was about 400% higher than the 1909 event (GRACE's case). This is explained by the likely impacts of several CMEs on the magnetosphere during the main and recovery phases of the March 1989 superstorm (Fujii

et al., 1992; Lakhina & Tsurutani, 2016; Boteler, 2019). Therefore, as opposed to latitudinal extent of aurorae, a superstorm with a smaller amplitude rate (absolute value) can cause more detrimental effects on orbital drag in comparison to an even stronger superstorms that develops faster (larger absolute value of amplitude rate). All orbital degradations shown in Table 1 are much more severe than the orbital degradation due to the background density estimated by Oliveira and Zesta (2019) during November 2003 for CHAMP (–34.45 m) and GRACE (–6.86 m); therefore, these results set a new basis for these effects. Despite the fact that these effects can have significant error levels particularly during the storm recovery phases due to the lack of nitric oxide cooling effects in the model (Mlynczak et al., 2003; Bowman et al., 2008; Knipp et al., 2017; Oliveira & Zesta, 2019; Zesta & Oliveira, 2019), these results reveal the comparative roles of time durations and strengths of magnetic superstorms in controlling drag effects.

The results of this work clearly show that multiple CME impacts on the Earth's magnetosphere (as in the March 1989 superstorm), particularly occurring during active times, can largely enhance satellite orbital drag due to long and sustained storm times. These drag effects can be more severe when compared to drag effects during storms caused by a single CME leading to even more intense storms, but lasting shorter. Therefore, orbital drag forecasters should be aware of potential impacts of several CMEs on the terrestrial magnetosphere during ongoing magnetic storms (e.g., Zhao & Dryer, 2014, and many references therein). In a future work, simulation results of tens of historical severe and extreme magnetic storms, with minimum Dst $\leq$ –250 nT excluding superstorms (Meng et al., 2019; Oliveira & Zesta, 2019; Zesta & Oliveira, 2019; Chapman et al., 2020), will be statistically studied.

References

Allen, J., Sauer, H., Frank, L., & Reiff, P. (1989). Effects of the March 1989 solar activity. *Eos Transactions AGU*, *70*(46), 1479–1488. https://doi.org/10.1029/89EO00409

Balan, N., Skoug, R., Tulasi Ram, S., Rajesh, P. K., Shiokawa, K., Otsuka, Y., ... Nakamura, T. (2014). CME front and severe space weather. *Journal of Geophysical Research: Space Physics*, *119*(12), 10,041-10,058. https://doi.org/10.1002/2014JA020151

Berger, T., Holzinger, M., Sutton, E., & Thayer, J. (2020). Flying Through Uncertainty. *Space Weather*, *18*. https://doi.org/10.1029/2019SW002373

Blake, S. P., Pulkkinen, A. A., & Schuck, P. W. (2019). Latitudinal Extent of the Auroral Oval during the Carrington Event. In *Final paper abstract number: IN41B-09*. Presented at 2019 AGU Fall Meeting, Washington, D.C., 10-14 Dec.

Bolduc, L. (2002). GIC observations and studies in the Hydro-Québec power system. *Journal of Atmospheric and Solar-Terrestrial Physics*, *64*(16), 1793-1802.

https://doi.org/10.1016/S1364-6826(02)00128-1

Boteler, D. H. (2019). A TwentyFirst Century View of the March 1989 Magnetic Storm. *Space Weather*, *17*(10), 1427-1441. https://doi.org/10.1029/2019SW002278

Bowman, B. R., Tobiska, W. K., Marcos, F. A., Huang, C. Y., Lin, C. S., & Burke, W. J. (2008). A new empirical thermospheric density model JB2008 using new solar and geomagnetic indices. In *AIAA/AAS Astrodynamics Specialist Conference, AIAA 2008–6438* (p. 1-19). Honolulu, HI.

Bruinsma, S. L., & Forbes, J. M. (2007). Global observations of traveling atmospheric disturbances (TADs) in the thermosphere. *Geophysical Research Letters*, *34*(L14103). https://doi.org/10.1029/2007GL030243

Bruinsma, S. L., Tamagnan, D., & Biancale, R. (2004). Atmospheric densities derived from CHAMP/STAR accelerometer observations. *Planetary and Space Science*, *62*(4), 297–312. https://doi.org/10.1016/j.pss.2003.11.004

Burke, W. J. (2018). Thermospheric Dynamics during the March 1989 Magnetic Storm. *Sun and Geosciences*, *13*(2), 163-168. https://doi.org/10.31401/SunGeo.2018.02.07

Chapman, S. C., Horne, R. B., & Watkins, N. W. (2020). Using the aa index over the last 14 solar cycles to characterize extreme geomagnetic activity. *Geophysical Research Letters*, *n/a*(n/a), e2019GL086524. doi: 10.1029/2019GL086524

Chen, G.-m., Xu, J., Wang, W., Lei, J., & Burns, A. G. (2012). A comparison of the effects of CIR– and CME–induced geomagnetic activity on thermospheric densities and spacecraft orbits: Case studies. *Journal of Geophysical Research*, *117*(A8). https://doi.org/10.1029/2012JA017782

Chree, C. (1921). The Magnetic Storm of 13-17 May. *Nature*, *107*(2690), 359. https://doi.org/10.1038/107359a0

Cliver, E. W., & Dietrich, W. F. (2013). The 1859 space weather event revisited: limits of extreme activity. *Journal of Space Weather and Space Climate*, *3*(A31). https://doi.org/10.1051/swsc/2013053

Connor, H. K., Zesta, E., Fedrizzi, M., Shi, Y., Raeder, J., Codrescu, M. V., & Fuller-Rowell, T. J. (2016). Modeling the ionosphere-thermosphere response to a geomagnetic storm using physics-based magnetospheric energy input: OpenGGCM-CTIM results. *Journal of Space Weather and Space Climate*, *6*(A25), 1–15. https://doi.org/10.1051/swsc/2016019

Daglis, I. A., Thorne, R. M., Baumjohann, W., & Orsini, S. (1999). The terrestrial ring current: Origin, formation, and decay. *Reviews of Geophysics*, *37*(4), 407-438. https://doi.org/10.1029/1999RG900009

Doornbos, E., & Klinkrad, H. (2006). Modelling of space weather effects on satellite drag. *Advances in Space Research*, *37*(6), 1229–1239. https://doi.org/10.1016/j.asr.2005.04.097

Emmert, J. T. (2015). Thermospheric mass density: A review. *Advances in Space Research*, *56*(5), 773–824. https://doi.org/10.1016/j.asr.2015.05.038

Flury, J., Bettadpur, S., & Tapley, B. D. (2008). Precise accelerometry onboard the GRACE gravity field satellite mission. *Advances in Space Research*, *42*(8), 1414-1423. https://doi.org/10.1016/j.asr.2008.05.004

Fujii, R., Fukunishi, H., Kokubun, S., Sugiura, M., Tohyama, F., Hayakawa, H., . . . Okada, T. (1992). Field-aligned current signatures during the March 1314, 1989, Great Magnetic Storm. *Journal of Geophysical Research*, *97*(A7), 10703-10715. https://doi.org/10.1029/92JA00171

Fuller-Rowell, T. J., Codrescu, M. V., Moffett, R. J., & Quegan, S. (1994). Response of the thermosphere and ionosphere to geomagnetic storms. *Journal of Geophysical Research*, *99*(A3), 3893–3914. https://doi.org/10.1029/93JA02015

Gonzalez, W. D., Joselyn, J. A., Kamide, Y., Kroehl, H. W., Rostoker, G., Tsurutani, B. T., & Vasyliūnas, V. M. (1994). What is a geomagnetic storm? *Journal of Geophysical Research*, *99*(A4), 5771–5792.

https://doi.org/10.1029/93JA02867

Hapgood, M. (2019). The Great Storm of May 1921: An Exemplar of a Dangerous Space Weather Event. *Space Weather*, *17*(7), 950-975. https://doi.org/10.1029/2019SW002195

Hayakawa, H., Ebihara, Y., Cliver, E. W., Hattori, K., Toriumi, S., Love, J. J., ... Shibata, K. (2019). The extreme space weather event in September 1909. *Monthly Notes of the Royal Astrononomical Society*, *484*(3), 4083-4099. https://doi.org/10.1093/mnras/sty3196

Hayakawa, H., Ebihara, Y., Willis, D. M., Toriumi, S., Iju, T., Hattori, K., ... Knipp, D. J. (2019). Temporal and Spatial Evolutions of a Large Sunspot Group and Great Auroral Storms around the Carrington Event in 1859. *Space Weather*, *17*(11), 1553-1569. https://doi.org/10.1029/2019SW002269

Hayakawa, H., Ribeiro, P., Vaquero, J. M., Gallego, M. C., Knipp, D. J., Mekhaldi, F., ... Ebihara, Y. (2020). The Extreme Space Weather Event in 1903 October/November: An Outburst from the Quiet Sun. *The Astrophysical Journal Letters*, *888*(2). https://doi.org/10.3847/2041-8213/ab6a18

He, C., Yang, Y., Carter, B., Kerr, E., Wu, S., Deleflie, F., ... Norman, R. (2018). Review and comparison of empirical thermospheric mass density models. *Progress in Aerospace Sciences*, *103*, 31-51. https://doi.org/10.1016/j.paerosci.2018.10.003

Hocke, K., & Schlegel, K. (1996). A review of atmospheric gravity waves and travelling ionospheric disturbances: 1982–1995. *Annales Geophysicae*, *14*(9), 917–940. doi: 10.1007/s00585-996-0917-6

Huang, C. Y., Su, Y.-J., Sutton, E. K., Weimer, D. R., & Davidson, R. L. (2014). Energy coupling during the August 2011 magnetic storm. *Journal of Geophysical Research: Space Physics*, *119*(2), 1219–1232. https://doi.org/10.1002/2013JA019297

Jonas, S., Murtagh, W., & Bonadonna, M. (2017). Released for Public Comment: Space Weather Benchmarks and Operations-to-Research Plan. *Space Weather*, *15*(2), 282-282. https://doi.org/10.1002/2017SW001603

Joselyn, J. A. (1990). Case study of the great geomagnetic storm of 13 March 1989, Astrodynamics 1989. In *Proceedings of the AAS/AIAA Astrodynamics Conference, Stowe, VT, August 7-10, 1989* (p. 745-762). San Diego, CA: Univelt, Inc. (Part 2 (A9046754 2112))

Kalafatoglu Eyiguler, E. C., Kaymaz, Z., Frissell, N. A., Ruohoniemi, J. M., & Rastätter, L. (2018). Investigating upper atmospheric Joule heating using cross-combination of data for two moderate substorm cases. *Space Weather*, *16*(8), 987-1012. https://doi.org/10.1029/2018SW001956

Kappenman, J. G. (2006). Great geomagnetic storms and extreme impulsive geomagnetic field disturbance events - An analysis of observational evidence including the great storm of May 1921. *Advances in Space Research*, *38*(2), 188-199. https://doi.org/10.1016/j.asr.2005.08.055

Kilpua, E. K. J., Fontaine, D., Moissard, C., Ala-Lahti, M., Palmerio, E., Yordanova, E., ... Turc, L. (2019). Solar Wind Properties and Geospace Impact of Coronal Mass Ejection-Driven Sheath Regions: Variation and Driver Dependence. *Space Weather*, *17*(8), 1257-1280. https://doi.org/10.1029/2019SW002217

Knipp, D. J., Pette, D. V., Kilcommons, L. M., Isaacs, T. L., Cruz, A. A., Mlynczak, M. G., ... Lin, C. Y. (2017). Thermospheric nitric oxide response to shock-led storms. *Space Weather*, *15*(2), 325-342. https://doi.org/10.1002/2016SW001567

Krauss, S., Temmer, M., & Vennerstrom, S. (2018). Multiple satellite analysis of the Earth's thermosphere and interplanetary magnetic field variations due to ICME/CIR events during 2003-2015. *Journal of Geophysical Research: Space Physics*, *123*(10), 8884-8894. https://doi.org/10.1029/2018JA025778

Krauss, S., Temmer, M., Veronig, A., Baur, O., & Lammer, H. (2015). Thermosphere and geomagnetic response to interplanetary coronal mass ejections observed by ACE and GRACE: Statistical results. *Journal of Geophysical Research: Space Physics*, *120*(10), 8848–8860. https://doi.org/10.1002/2015JA021702

Lakhina, G. S., & Tsurutani, B. T. (2016). Geomagnetic storms: Historical perspective to modern view. *Geoscience Letters*, *3*(5), 1–11. https://doi.org/10.1186/s40562-016-0037-4

Lanzerotti, L. J. (2015). Space Weather Strategy and Action Plan: The National Program Is Rolled Out. *Space Weather*, *13*(12), 824-825. https://doi.org/10.1002/2015SW001334

Liu, H., & Lühr, H. (2005). Strong disturbance of the upper thermospheric density due to magnetic storms: CHAMP observations. *Journal of Geophysical Research*, *110*(A9), 1–9. https://doi.org/10.1029/2004JA010908

Liu, H., Lühr, H., Henize, V., & Köhler, W. (2005). Global distribution of the thermospheric total mass density derived from CHAMP. *Journal of Geophysical Research*, *110*(A4). https://doi.org/10.1029/2004JA010741

Lockyer, W. J. S. (1903). Magnetic Storms, AurorÆ and Solar Phenomena. *Nature*, *69*(1775), 9-10. https://doi.org/10.1038/069009a0

Love, J. J., Hayakawa, H., & Cliver, E. W. (2019a). Intensity and impact of the New York Railroad superstorm of May 1921. *Space Weather*, *17*(8), 1281-1292. https://doi.org/10.1029/2019SW002250

Love, J. J., Hayakawa, H., & Cliver, E. W. (2019b). On the Intensity of the Magnetic Superstorm of September 1909. *Space Weather*, *17*(1), 37-45. https://doi.org/10.1029/2018SW002079

Lu, G., Richmond, A. D., Lühr, H., & Paxton, L. (2016). High-latitude energy input and its impact on the thermosphere. *Journal of Geophysical Research: Space Physics*, *121*(7), 7108–7124. https://doi.org/10.1002/2015JA022294

Meng, X., Tsurutani, B. T., & Mannucci, A. J. (2019). The Solar and Interplanetary Causes of Superstorms (Minimum Dst $\leq$ –250 nT) During the Space Age. *Journal of Geophysical Research: Space Physics*, *124*(6), 3926-3948. https://doi.org/10.1029/2018JA026425

Mlynczak, M. G., Martin-Torres, F. J., Russell, J., Beaumont, K., Jacobson, S., Kozyra, J., . . . Paxton, L. (2003). The natural thermostat of nitric oxide emission at 5.3 μm in the thermosphere observed during the solar storms of April 2002. *Geophysical Research Letters*, *30*(21). https://doi.org/10.1029/2003GL017693

Moe, K., & Moe, M. M. (2005). Gas-surface interactions and satellite drag coefficients. *Planetary and Space Science*, *53*(8), 793-801. https://doi.org/10.1016/j.pss.2005.03.005

National Science and Technology Council. (2015b). *National Space Weather Strategy* (Tech. Rep.). Washington, D.C.: Executive Office of the President of the United States. Retrieved from `https://obamawhitehouse` `.archives.gov/sites/default/files/microsites/ostp/final` `_nationalspaceweatherstrategy_20151028.pdf`

National Science and Technology Council. (2015a). *National Space Weather Action Plan* (Tech. Rep.). Washington, D.C.: Executive Office of the President of the United States. Retrieved from `https://obamawhitehouse` `.archives.gov/sites/default/files/microsites/ostp/final` `_nationalspaceweatheractionplan_20151028.pdf`

Oliveira, D. M., Arel, D., Raeder, J., Zesta, E., Ngwira, C. M., Carter, B. A., . . . Gjerloev, J. W. (2018). Geomagnetically induced currents caused by interplanetary shocks with different impact angles and speeds. *Space Weather*, *16*(6), 636-647. https://doi.org/10.1029/2018SW001880

Oliveira, D. M., & Ngwira, C. M. (2017). Geomagnetically Induced

Currents: Principles. *Brazilian Journal of Physics*, *47*(5), 552-560. https://doi.org/10.1007/s13538-017-0523-y

Oliveira, D. M., & Zesta, E. (2019). Satellite Orbital Drag During Magnetic Storms. *Space Weather*, *17*(11), 1510-1533. https://doi.org/10.1029/2019SW002287

Oliveira, D. M., Zesta, E., Schuck, P. W., & Sutton, E. K. (2017). Thermosphere global time response to geomagnetic storms caused by coronal mass ejections. *Journal of Geophysical Research: Space Physics*, *122*(10), 10,762-10,782. https://doi.org/10.1002/2017JA024006

Page, J. (1903). The Polar Aurora of October 30 – November 1, 1903. *Monthly Weather Review*, *31*(12), 592-593. https://doi.org/0.1175/1520-0493(1903)31[592c:TPAOON]2.0.CO;2

Prieto, D. M., Graziano, B. P., & Roberts, P. C. E. (2014). Spacecraft drag modelling. *Progress in Aerospace Sciences*, *64*, 56-65. https://doi.org/10.1016/j.paerosci.2013.09.001

Prölss, G. (2011). Density perturbations in the upper atmosphere caused by the dissipation of solar wind energy. *Surveys in Geophysics*, *32*(2), 101–195. https://doi.org/10.1007/s10712-010-9104-0

Pulkkinen, A., Bernabeu, E., Eichner, J., Beggan, C., & Thomson, A. W. P. (2012). Generation of 100-year geomagnetically induced current scenarios. *Space Weather*, *10*(4). doi: 10.1029/2011SW000750

Pulkkinen, A., Bernabeu, E., Thomson, A., Viljanen, A., Pirjola, R., Boteler, D., . . . MacAlester, M. (2017). Geomagnetically induced currents: Science, engineering, and applications readiness. *Space Weather*, *15*(7), 828-856. https://doi.org/10.1002/2016SW001501

Richmond, A., & Lu, G. (2000). Upper-atmospheric effects of magnetic storms: A brief tutorial. *Journal of Atmospheric and Solar-Terrestrial Physics*, *62*(12), 1115-1127. https://doi.org/10.1016/S1364-6826(00)00094-8

Reigber, C., Lühr, H., & Schwintzer, P. (2002). CHAMP mission status. *Advances in Space Research*, *30*(2), 129-134. https://doi.org/10.1016/S0273-1177(02)00276-4

Ribeiro, P., Vaquero, J. M., Gallego, M. C., & Trigo, R. M. (2016). The First Documented Space Weather Event That Perturbed the Communication Networks in Iberia. *Space Weather*, *14*(7), 464-468. https://doi.org/10.1002/2016SW001424

Rich, F. J., & Denig, W. F. (1992). The major magnetic storm of March 13-14, 1989 and associated ionosphere effects. *Canadian Journal of Physics*, *70*(7), 510-525. https://doi.org/10.1139/p92-086

Riley, P., Baker, D., Liu, Y. D., Verronen, P., Singer, H., & Güdel, M. (2018). Extreme Space Weather Events: From Cradle to Grave. *Space Science Reviews*, *214*(21). https://doi.org/10.1007/s11214-017-0456-3

Shepherd, S. G. (2014). Altitude-adjusted corrected geomagnetic coordinates: Definition and functional approximations. *Journal of Geophysical Research: Space Physics*, *119*(9), 7501–7521. https://doi.org/10.1002/2014JA020264

Shi, Y., Oliveira, D. M., Knipp, D. J., Zesta, E., Matsuo, T., & Anderson, B. (2019). Effects of Nearly Frontal and Highly Inclined Interplanetary Shocks on High-latitude Field-aligned Currents (FACs). *Space Weather*, *17*(12), 1659-1673. https://doi.org/10.1029/2019SW002367

Silverman, S. M. (1995). Low latitude auroras: the storm of 25 September 1909. *Journal of Atmospheric and Solar-Terrestrial Physics*, *57*(6), 673-685. https://doi.org/10.1016/0021-9169(94)E0012-C

Silverman, S. M., & Cliver, E. W. (2001). Low-latitude auroras: the magnetic storm of 14-15 May 1921. *Journal of Atmospheric and Solar-Terrestrial Physics*, *63*(5), 523-535. https://doi.org/10.1016/S1364-6826(00)00174-7

Siscoe, G., Crooker, N. U., & Clauer, C. R. (2006). Dst of the Carrington storm of 1859. *Advances in Space Research*, *38*(2), 173-179.

https://doi.org/10.1016/j.asr.2005.02.102

Sugiura, M. (1964). Hourly values of equatorial Dst for the IGY. *Ann. Int. Geophys. Year*, *35*(5).

Sutton, E. K. (2009). Normalized force coefficients for satellites with elongated shapes. *Journal of Spacecraft and Rockets*, *46*(1), 112–116. https://doi.org/10.2514/1.40940

Sutton, E. K., Forbes, J. M., & Knipp, D. J. (2009). Rapid response of the thermosphere to variations in Joule heating. *Journal of Geophysical Research*, *114*(A4). https://doi.org/10.1029/2008JA013667

Tapley, B. D., Bettadpur, S., Watkins, M., & Reigber, C. (2004). The gravity recovery and climate experiment: Mission overview and early results. *Geophysical Research Letters*, *31*(9). https://doi.org/10.1029/2004GL019920

Tsurutani, B. T., Gonzalez, W. D., Lakhina, G. S., & Alex, S. (2003). The extreme magnetic storm of 1-2 September 1859. *Journal of Geophysical Research*, *108*(A7). https://doi.org/10.1029/2002JA009504

Tsurutani, B. T., Verkhoglyadova, O. P., Mannucci, A. J., Araki, T., Sato, A., Tsuda, T., & Yumoto, K. (2007). Oxygen ion up-lift and satellite drag effects during the 30 October 2003 daytime superfountain event. *Annales Geophysicae*, *25*, 569574. https://doi.org/10.5194/angeo-25-569-2007

Tsurutani, B. T., & Lakhina, G. S. (2014). An extreme coronal mass ejection and consequences for the magnetosphere and Earth. *Geophysical Research Letters*, *41*(2), 287-292. https://doi.org/10.1002/2013GL058825

Vennerstrøm, S., Lefévre, L., Dumbović, M., Crosby, N., Malandraki, O., Patsou, I., Clette, F., Veronig, A., Vršnak, B., Leer, K., & Moretto, T. (2016). Extreme geomagnetix storms - 1868 - 2010. *Solar Physics*, *291*(5), 1447-1481. https://doi.org/10.1007/s11207-016-0897-y

World Data Center for Geomagnetism, Kyoto, Nose, M., Iyemori, T., Sugiura, M., & Kamei, T. (2015). *Geomagnetic Dst index*. https://doi.org/10.17593/14515-74000

Zesta, E., & Huang, C. Y. (2016). Satellite orbital drag. In G. V. Khazanov (Ed.), *Space Weather Fundamentals* (pp. 329–351). Boca Raton, FL: CRC Press.

Zesta, E., & Oliveira, D. M. (2019). Thermospheric heating and cooling times during geomagnetic storms, including extreme events. *Geophysical Research Letters*, *46*(22), 12,739-12,746. https://doi.org/10.1029/2019GL085120

Zhao, X., & Dryer, M. (2014). Current status of CME/shock arrival time prediction. *Space Weather*, *12*(7), 448-469. doi: 10.1002/2014SW001060

Figure 1.

Standard (Dst) and alternative (Dst†) disturbance storm time stations
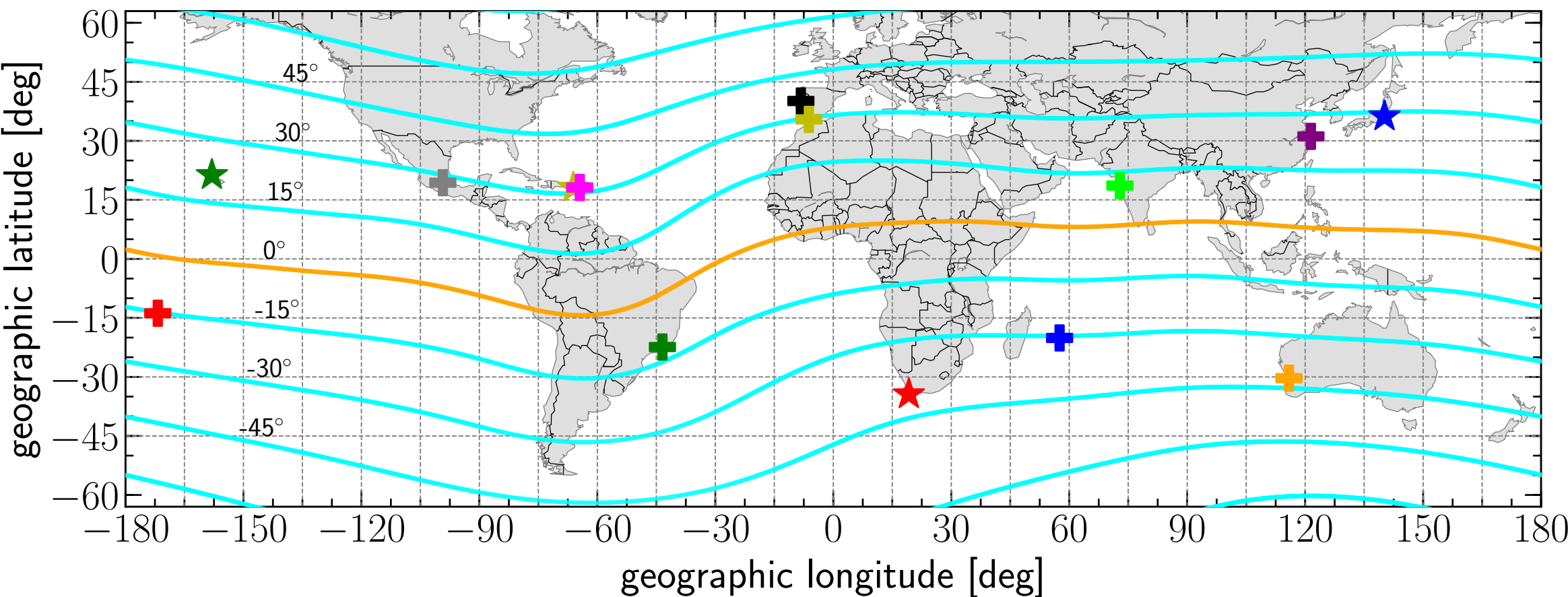
Standard Dst stations

★ Honolulu [HON], United States

★ San Juan [SJG], Puerto Rico

★ Hermanus [HER], South Africa

★ Kakioka, [KAK], Japan

Magnetic coordinates for 1957

▬ Magnetic latitudes

▬ Magnetic equator

Alternative Dst† stations

✚ Apia [API], Western Samoa (1909, 1921)

✚ Coimbra [COI], Portugal (1903)

✚ Colaba [CLA], India (1903)

✚ Cuajimalpa [CUA], Mexico (1903)

✚ Mauritius [MRI], Mauritius (1909)

✚ San Fernando [SFS], Spain (1909, 1921)

✚ Vassouras [VSS], Brazil (1921)

✚ Vieques [VQS], Puerto Rico (1909)

✚ Watheroo [WAT], Australia (1921)

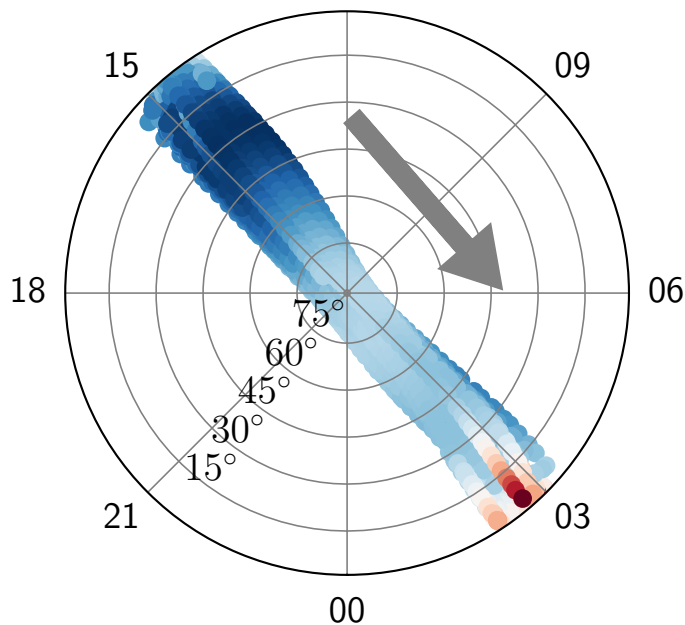✚ Zi-Ka-Wei [ZKW], China (1903)

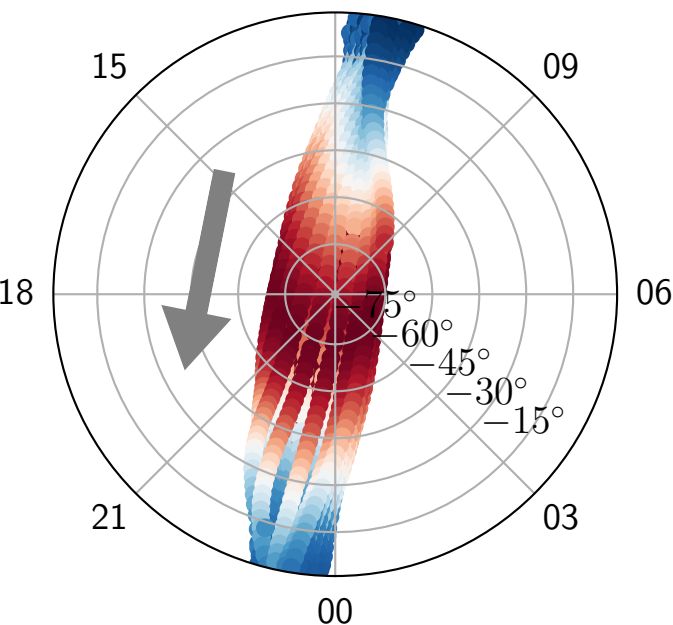**Figure 2.**

CHAMP
Northern Hemisphere
12 MLT
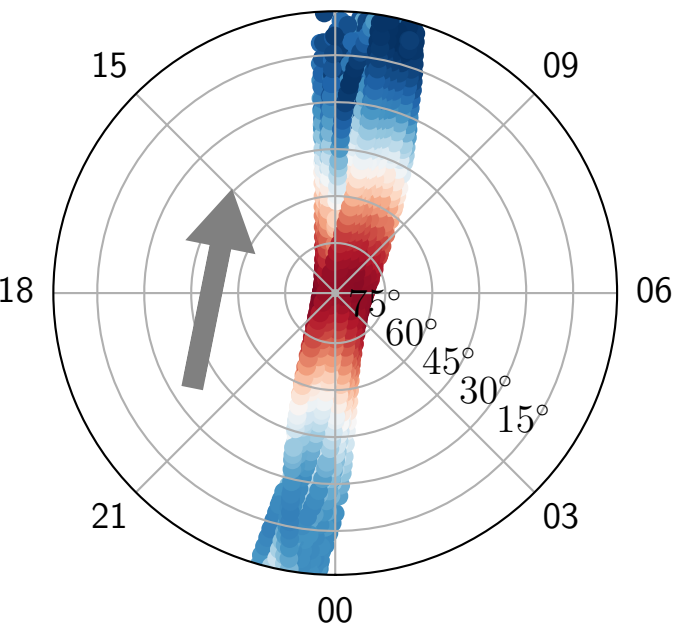
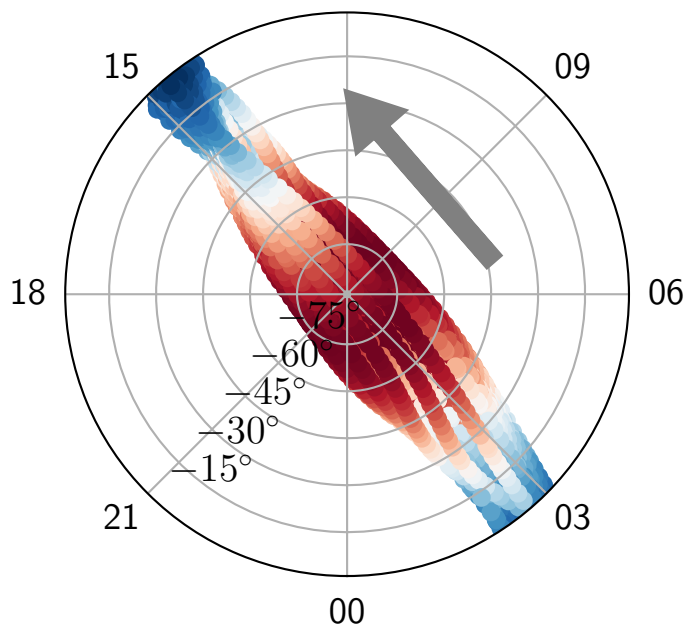GRACE
Northern Hemisphere
12 MLT

Southern Hemisphere
12 MLT

Southern Hemisphere
12 MLT

CHAMP altitude [km]

GRACE altitude [km]

Figure 3.

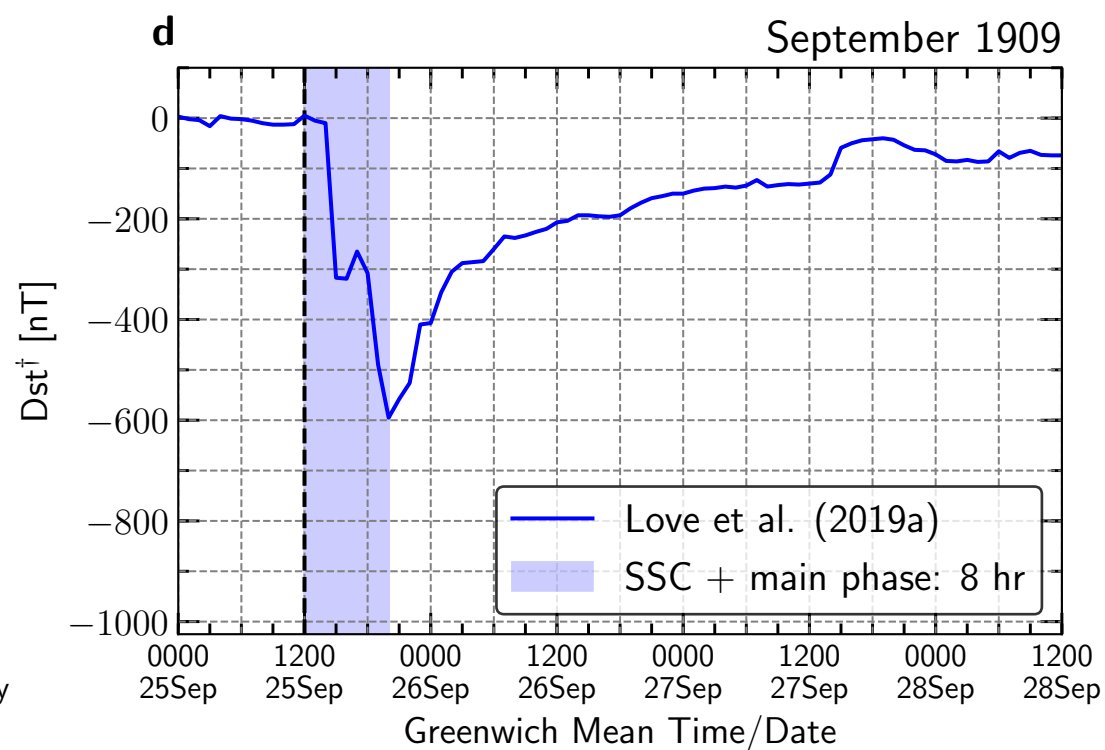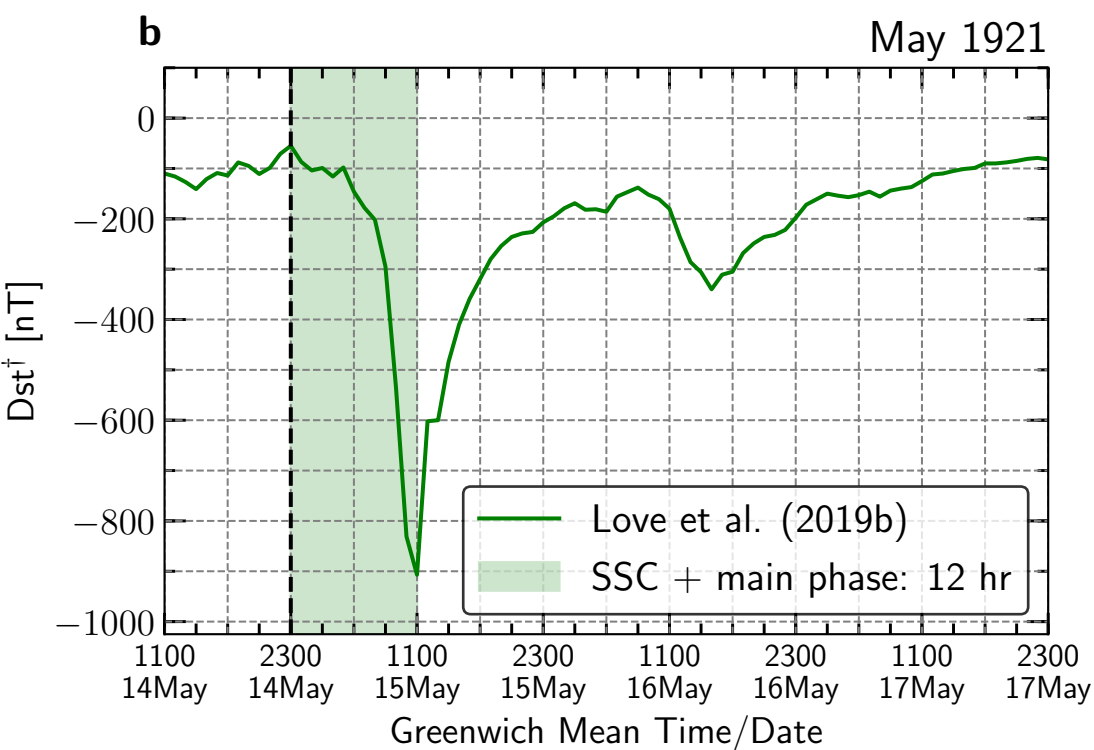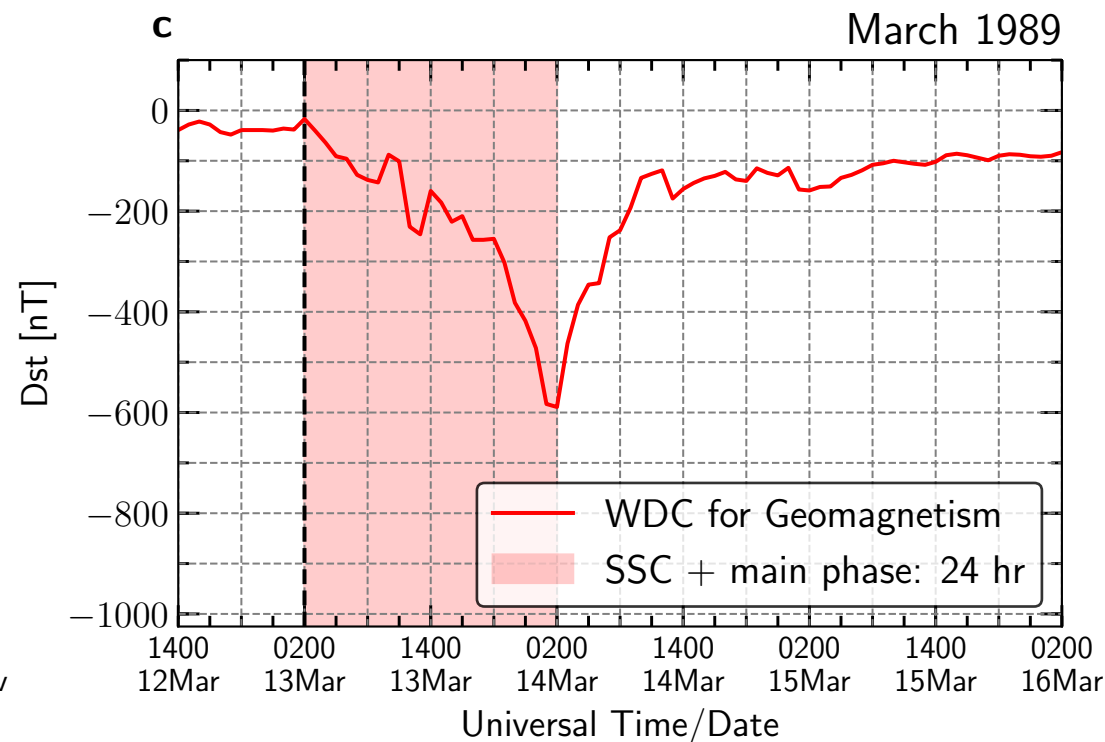# Dst (standard) and Dst† (alternative) indices for the selected magnetic superstorms

a October/November 1903

Dst† [nT]

Legend:
- Hayakawa et al. (2020)
- SSC + main phase: 14 hr

Greenwich Mean Time/Date

b May 1921

Dst† [nT]

Legend:
- Love et al. (2019b)
- SSC + main phase: 12 hr

Greenwich Mean Time/Date

c March 1989

Dst† [nT]

Legend:
- WDC for Geomagnetism
- SSC + main phase: 24 hr

Universal Time/Date

d September 1909

Dst† [nT]

Legend:
- Love et al. (2019a)
- SSC + main phase: 8 hr

Greenwich Mean Time/Date
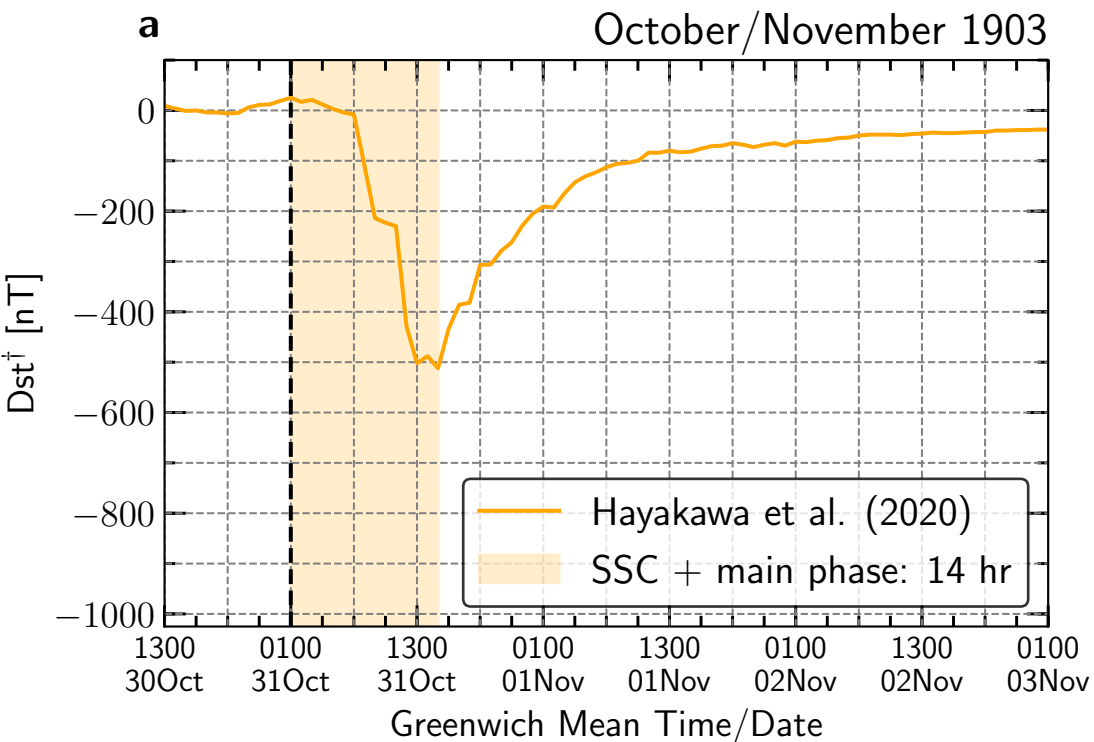
Figure 4.

Storm-time orbital drag effects for CHAMP's orbit

a1   Orbital decay rate
            c1   Orbital decay rate

b1   Orbital decay
            d1   Orbital decay
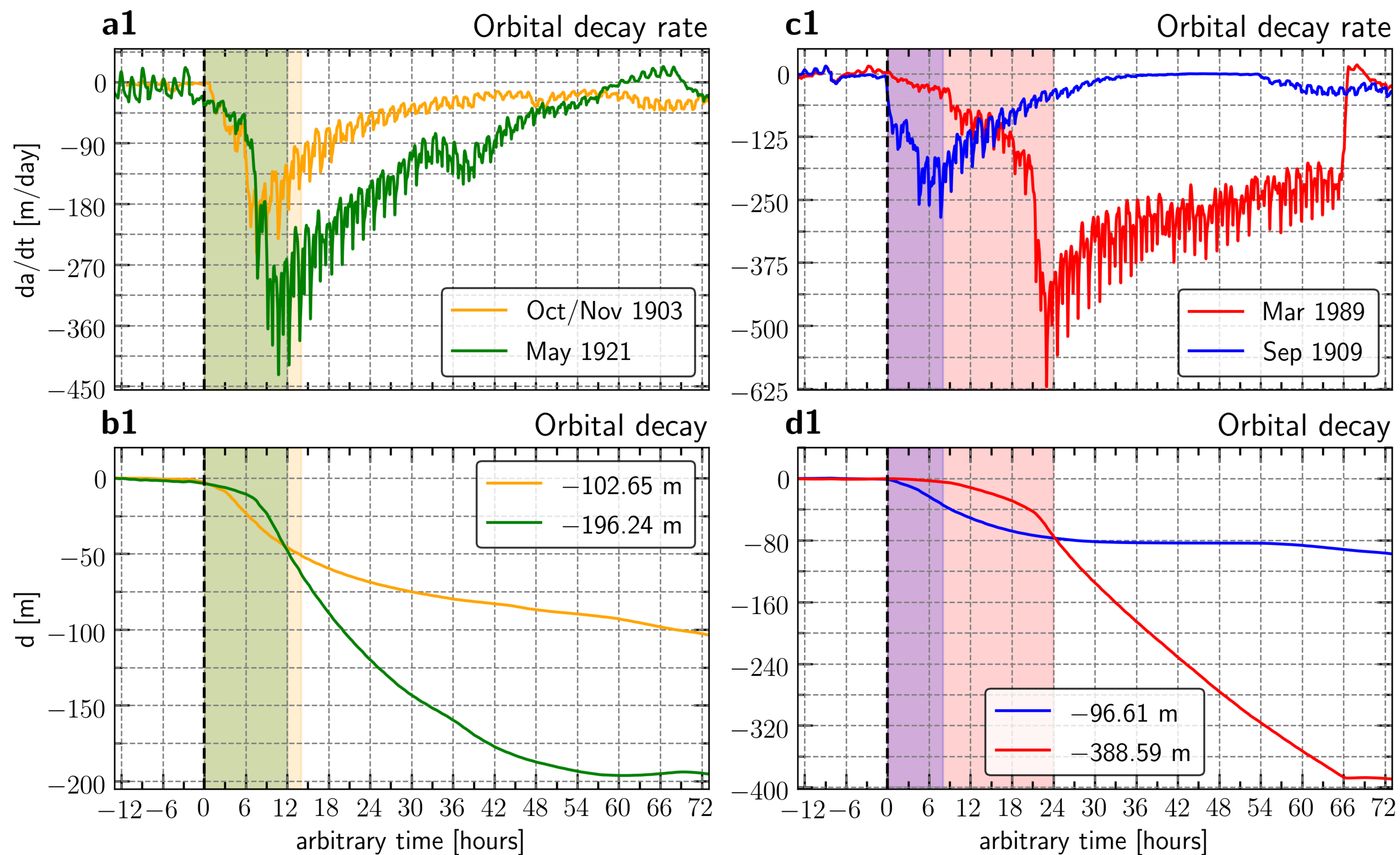
Storm-time orbital drag effects for GRACE's orbit

a2   Orbital decay rate
            c2   Orbital decay rate

b2   Orbital decay
            d2   Orbital decay